ELSEVIER

Contents lists available at ScienceDirect

Materials Today Physics

journal homepage: https://www.journals.elsevier.com/ materials-today-physics



Phase transformation via atomic-scale periodic interfacial energy



Ye Cui ^a, Yang Zhang ^a, Lixin Sun ^a, Mikhail Feygenson ^b, Mingyu Fan ^a, Xun-Li Wang ^c, Peter K. Liaw ^d, Ian Baker ^e, Zhongwu Zhang ^{a,*}

- ^a Key Laboratory of Superlight Materials and Surface Technology, Ministry of Education, College of Materials Science and Chemical Engineering, Harbin, Engineering University, Harbin, 150001, China
- ^b Forschungszentrum Jülich GmbH, Jülich Centre for Neutron Science (JCNS-1) and Biological Matter (IBI-8), 52425, Jülich, Germany
- ^c Department of Physics, City University of Hong Kong, 83 Tat Chee Avenue, Kowloon, Hong Kong
- d Department of Materials Science and Engineering, The University of Tennessee, Knoxville, TN, 37996-2100, USA
- ^e Thayer School of Engineering, Dartmouth College, 14 Engineering Drive, Hanover, NH, 03755, USA

ARTICLE INFO

Article history: Received 14 January 2022 Received in revised form 5 March 2022 Accepted 14 March 2022 Available online 18 March 2022

Keywords:
Diffusional transformation
Displacive transformation
Interfacial energy
Mg—Li alloy
Neutron total scattering

ABSTRACT

Displacive and diffusional transformations are the main processes during solid-state phase transformations, which have formed the basis of applied physics and materials technology for centuries. However, the relationship between diffusional and displacive transformations has remained elusive, which significantly hinders the fundamental understanding and control of the microstructures and properties of materials via phase transformations. Here, we introduce the concept of a periodic differential interfacial energy between atom layers. We develop the mechanism of an atomic-scale displacive process in the form of atoms groups (cells) based on the periodic differential interfacial energy and experimentally determine the displacive short-range order (SRO) cell size in an Mg—Li alloy using a neutron total scattering method. We proposed that the origins of both the displacive and diffusional transformations are displacive in nature governed by the driving force of transformations. Our work paves the way for building a bridge correlating the nature of various solid-state phase transformations.

1. Introduction

Understanding the thermodynamics and kinetics of solid-state phase (s-s) transformations is one of the most fundamental issues in materials science, and is critical in engineering the crystallographic [1–3], mechanical [4–7], and physical properties [8,9] of materials. In general, s-s transformations are classified into two types: diffusional and displacive. A diffusional transformation is a thermally-activated process, which is considered to occur by means of the random walk of individual atoms through thermal activation [10]. A displacive transformation is a diffusionless transformation that occurs through shearing and shuffling of a group of atoms without thermal activation after nucleation. However, the correlation between diffusional and displacive transformations is still one of the few remaining uncertainties in understanding s-s transformations.

Although many transformations produce surface relief effects involving compositional changes [11], which may bridge the gap

* Corresponding author.

E-mail address: zwzhang@hrbeu.edu.cn (Z. Zhang).

between diffusional and displacive transformations, the nature of these displacive processes accompanied by atom diffusion has been argued about for more than a century [12,13]. To date, the most important theory of transformations is classical nucleation theory (CNT) [14,15]. However, this explains the transformation process without fully considering the effects of interfacial structure on the atomic scale. It is worth noting that it is also quite difficult to experimentally characterize the atomic structure by conventional diffraction, spectroscopic, or imaging techniques [16].

Here, we introduce the concept of a periodic differential interfacial energy between atom layers. The atomic-scale correlation of displacive and diffusional transformations with the competition between the periodic interfacial energy and driving force, determined by the composition and crystal structure, is of fundamental interest and provides an ideal platform for studying the nature of different transformations with various interfacial structures. A dual-phase binary Mg—Li alloy was selected as a representative sample for the experimental part of our work. The interfacial structure phase of this alloy is well established by transmission electron microscopy (TEM) [17]. Pair-distribution function (PDF) studies were carried out to assess the local crystal structure of

Mg—Li on the atomic scale. A powerful combination of TEM with synchrotron x-ray and neutron PDF measurements [18—21] provided experimental evidence for the proposed theory. Critical insights for understanding diffusion and diffusionless transformations on an atomic scale are described.

2. Material and methods

2.1. Alloy preparation

The Mg–Li alloy ingots used in this study were prepared in a vacuum-induction furnace under argon by induction-melting high-purity elemental metals (99.9% Mg and 99.9% Li⁷ isotope in weight percent), followed by drop-casting into plates in a copper mold. Three compositions with different Li contents were prepared for comparison. The Li contents of these alloys are 3 wt percent (wt.%) (10 at.% Li, single α phase), 8 wt% (23 at.%, duplex phases), and 14 wt % (36 at.%, single β phase), respectively.

The as-cast buttons were encapsulated and annealed at 500 °C for 120 min and then quenched in water. This quenching process produces supersaturation of the β phase in the duplex alloy. Subsequently, the as-quenched samples were aged at 200 °C for 12 h to promote the precipitation of the α phase in Mg-8 wt. % Li. Then we collected the X-ray/neutron total scattering data during the α phase precipitation to evaluate the process.

2.2. Pair distribution function (PDF) characterization

Synchrotron X-ray total scattering data were collected at the 11-ID-B beamline of the Advanced Photon Source (APS), Argonne National Laboratory (ANL). Neutron data were collected at the Nanoscale-Ordered Materials Diffractometer (NOMAD) beamline [22] located at the Spallation Neutron Source (SNS), Oak Ridge National Laboratory (ORNL). The alloy button samples were loaded into polyimide capillaries and measured at ambient temperature. Data for an empty capillary were also collected. The normalized structure factor, S(Q), and subsequent PDFs were produced [22]. The X-ray PDFs were obtained, employing PDFgetX2 [23]. Q_{max} of 23.5 Å $^{-1}$ and 20 Å $^{-1}$ were used to obtain PDFs via a sine Fourier transition of S(Q) for x-ray and neutron data, respectively. The PDF data were segmentally refined with a box-car approach, employing the r-window of 10 Å. The refinements were done, using PDFgui software [24].

2.3. Scanning electron microscopy (SEM) characterization

The structures of the alloys were observed using scanning electron microscopy, SEM (JEOL MSM- 7800F). The SEM samples were mechanically polished and etched in a 4 vol percent (vol. %) nital solution, and then argon ion-polished to obtain strain free surface [25].

3. Theory

3.1. Periodic interface structure and energy

In CNT, the Gibbs free energy (G) of the transformation growth is described as follows: $\Delta G = -V \Delta G_V + A \gamma + V \Delta G_s$, where V is the volume of the new phase, A is the interfacial area of the phase, and γ is the specific interfacial energy [1,2,14]. ΔG_V describes the decrease in the Gibbs free energy per unit volume of the system during the transformation, and ΔG_s describes the change in the elastic strain energy. In general, the specific interfacial energy, γ , is always considered to be constant during the transformation. Here we introduce the concept of a periodic differential interfacial

energy determined by the atomic layer misfit between the new (α) and the parent (β) phases, as shown in Fig. 1a. Thus, the Gibbs free energy can be modified to be $\Delta G = -V(\Delta G_V - \Delta G_S) + \sum A_i \gamma_i$.

For simplicity, we first consider a one-dimensional transformation condition with the transformation direction along l_n (Fig. 1a). A new α phase is assumed to be a rectangle with a constant height of a and width of b during transformation. Thus, the free energy can be modified to,

$$\Delta G = -abl_n(\Delta G_V - \Delta G_S) + 2(a+b)d_\alpha \sum \gamma_i$$
 (1)

where l_n is the transformation length of the new phase, and d_α is the unstressed interplanar atom period spacing of matching planes in an α phase. Then this equation can be converted to the integral of the transformation length, l_n :

$$\Delta G = -abl_n(\Delta G_V - \Delta G_S) + 2(a+b) \int_0^{l_n} \gamma_l dl$$
 (2)

The first term, $abl_n(\Delta G_V - \Delta G_s) = \Delta G_d$, is the nominal transformation driving force. The second term, $2(a+b)\int\limits_0^{l_n}\gamma_Idl = \Delta G_i$, is the interfacial energy, originating from the periodic interfacial structure, which can be regarded as the nominal transformation-resistance factor.

We then consider the typical diffusional transformation with a

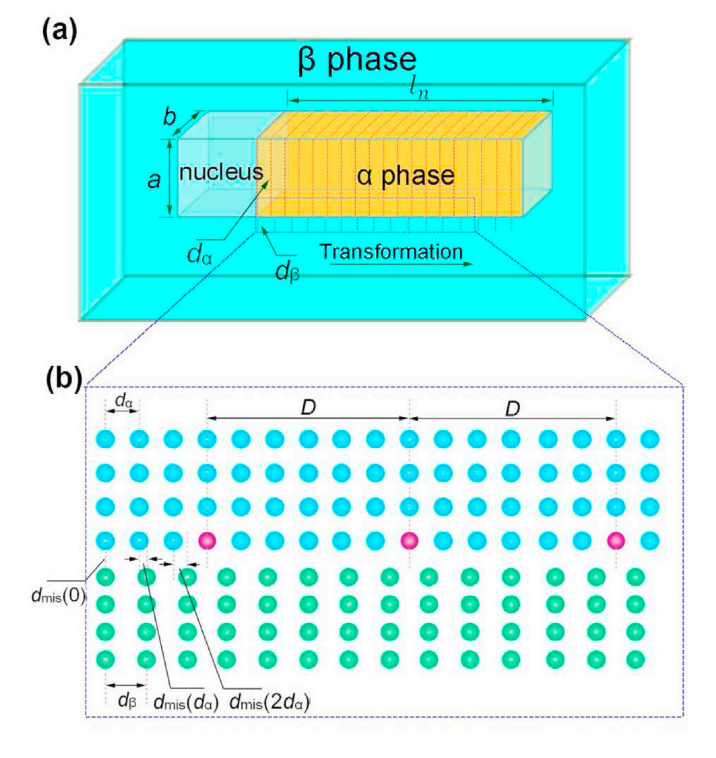


Fig. 1. Schematic of one-dimensional transformation. (a) Schematic of a partially-coherent interface without a rotated plane. (b) The relation of the atom is misfits $(d_{\rm mis})$ and matching planes. The value of a period misfit, $d_{\rm mis}$, was selected to be equal to an interplanar spacing of the matching planes. Some atoms on the interface are arranged at high interfacial energy sites (purple positions). They build up energy barriers, which prevent the spontaneous growth of a precipitated phase. The d_α and d_β is the unstressed interplanar atom period spacing of matching planes in an α phase and β phase, respectively. The $d_{\rm mis}(l)$ is the atom misfit of the atom layer, l. (For interpretation of the references to color in this figure legend, the reader is referred to the Web version of this article.)

semi-coherent interface. The semi-coherent interfacial energy can be approximately considered as a sum of two parts: a chemical contribution term, σ_{ic} , and a structural term, σ_{is} . Here, we assume that the dominant factor of the interfacial energy arises from atomic misfit at the interface. Based on the theory of linear elasticity, the differential interfacial energy from the atom-layer misfit can be expressed as [26]:

$$\gamma(l) = k[d_{mis}(l)]^2 \tag{3}$$

where k is a constant, which mainly depends on the elastic modulus of the new phase, and $d_{mis}(l)$ is the atomic misfit of the lth atom layer (Fig. 1b). From Eqs. (2) and (3), we have,

$$\Delta G = -abl_n(\Delta G_V - \Delta G_S) + 2(a+b) \int_0^{l_n} k[d_{mis}(l)]^2 dl$$
(4)

The lattice misfit of the semi-coherent interfaces can be completely accommodated without any long-range strain field by a set of edge dislocations, (Fig. 1b), because it has no rotational plane in one dimension. $d_{mis}(l)$ of the semicoherent interface has periodicity [10,27], which leads to a periodic differential interfacial energy, $\gamma(l)$, with a periodicity length of D, which is given by:

$$D = \frac{d_{\alpha}d_{\beta}}{|d_{\beta} - d_{\alpha}|} \tag{5}$$

where d_{β} is the unstressed interplanar spacing of matching planes in the parent β phase. The atomic misfit of the atom layer, l, could be expressed as a periodic function:

$$d_{mis}(l) = \frac{\left| \left(d_{\alpha} - d_{\beta} \right) (l + p_0) \right|}{d_{\alpha}} ,$$

$$d_{mis}(l \pm mD) = d_{mis}(l) \left(\frac{D}{2} - p_0 \ge l \ge -\frac{D}{2} - p_0, \right)$$
 (6)

where m is an integer, and $p_0 = |d_{\alpha}d_{mis}(0)/(d_{\alpha}-d_{\beta})|$.

3.2. Phenomenology of an atomic-scale displacive process

To analyze the effects of periodic interfacial energy on the atomic-scale transformation process, a single-layer transformation driving force, $\Delta G_{\rm d}'$, and resistance, $\Delta G_{\rm i}'$, of the l_n th atom layer is obtained from the derivatives of $\Delta G_{\rm d}$ and $\Delta G_{\rm i}$ to l_n ,

$$\Delta G_{\rm d}' = ab(\Delta G_{\rm V} - \Delta G_{\rm S}) \tag{7}$$

$$\Delta G_{i}'(l_{n}) = 2(a+b)k[d_{mis}(l_{n})]^{2}$$
(8)

 $\Delta G_{\rm i}'$, is a periodic function of l_n , while $\Delta G_{\rm d}'$, is independent of l_n . There are two extrema points with one periodicity, D, corresponding to the local metastable position ($\Delta G'=0$ and $\Delta G''>0$) and energy-barrier position ($\Delta G'=0$ and $\Delta G''<0$), respectively. When the $\Delta G_{\rm d}'$ of the nth atom layer, falls into the range between the local metastable state and the energy barrier, i. e., $\Delta G_{\rm i}'$ max > $\Delta G_{\rm d}' > \Delta G_{\rm i}'$ min, the local transformation is determined by the periodic-energy barriers and the metastable state. In other words, the local transformation process depends on the interfacial structure and the periodic interfacial energy, with the criterion of $(d_{mis-max})^2 > [ab(\Delta G_V - \Delta G_s)]/[2(a+b)k] > 0$, where $d_{mis-max}$ is the maximum value of d_{mis} . Due to the existence of the periodic-energy

barriers, an extra driving force is required to overcome them. This extra driving force can come from the composition optimization through the thermally-activated diffusion of atoms in the transformation cell, which matches the energy-barrier periodicity. With the extra driving force, the phase transformation is now driven by a cell transforming from one metastable state to the next one via a displacive method. The periodic interfacial energy suppresses the diffusional transformation occurring layer-by-layer or atom-by-atom. The size and shape of the cells are dependent on the periodicity of the interfacial energy. It is worth noting that this phenomenon depends only on the periodic interfacial energy. It implies that the atomic-scale displacive transformation is a general process for the first-order s-s transformation process with the periodic interfacial energy.

4. Results

4.1. 1Atomic-scale structure of an Mg-Li alloy

To verify the phenomenology of the atomic-scale displacive process, an Mg-8 wt.% Li alloy was selected as a representative example. The alloy has a duplex structure consisting of an hexagonal-close-packed (HCP) structure (α phase) and bodycentered-cubic (BCC) structure (β phase) [28]. The α/β transformation is considered a typical diffusional transformation. In addition, the interfacial structure between the α and β phases in Mg-8wt.%Li is well understood [17], and is described by $\{\overline{2}\ 11\}_{bcc}//\{\overline{1}\ 100\}_{hcp}$ and [0 $\overline{1}\ 1]_{bcc}//[0001]_{hcp}$. The periodicity of the interface between two phases has been experimentally confirmed by TEM studies [17]. The periodic length can be calculated from Eq. (5), in which d_α and d_β are determined to be 5.54 Å ($d_{m\{\overline{1}\ 100\}}\times 2$) and 8.62 Å ($d_{p\{\overline{2}\ 11\}}\times 6$), respectively. Thus, the periodic length of the interface between α and β phases is calculated to be 15.5 Å.

Synchrotron x-ray and neutron total scattering techniques were applied to characterize the short-range order (SRO) [29,30] and the local atom distribution using a PDF method. Modelling of the PDF data allowed verification of the effects of the periodic interfacial structure on the α/β phase transformation process. A Li7 isotope was used as tracer atoms in the Mg-8wt.%Li alloy to avoid neutron-absorption problems, which in turn made the identification of the SRO structures much more reliable.

In order to determine the size of the SRO [29,30] structures in the Mg–Li alloy, the neutron PDF data was fitted by assuming a disordered structure with Mg and Li atoms occupying random lattice positions. The agreement between the model and data is excellent (the weighted residual factor, $R_{\rm W}=0.07$) for interatomic distances greater than 20 Å. However, the fit quality becomes progressively lower below 20 Å, showing the largest deviation ($R_{\rm W}=0.174$) in the region between 2.4 Å and 10 Å (Fig. 2a). It is a clear indication of a SRO configuration of Mg and Li atoms within a cell with a diagonal length of about 20 Å (more details in the supplementary material).

We quantified the structure of the SRO cell by fitting the PDF data in a low-r (atom pair distance)-region to different structural models. The detailed description and fitting results for other models are described in supplementary materials. Here, the best fit for r=2.4-10 Å is shown in Fig. 2b. The model assumes that Li atoms in the α phase of a binary Mg–Li alloy are located in the $\{01\ \overline{1}\ 1\}_{hcp}$ planes. There is a Li-rich layer for every three $\{01\ \overline{1}\ 1\}_{hcp}$ planes, as shown in Fig. 2c. Li atoms in the β phase of the binary Mg–Li alloy are located in the $\{001\}_{bcc}$ planes. There is a Li-rich layer for every three layers, as shown in Fig. 2d.

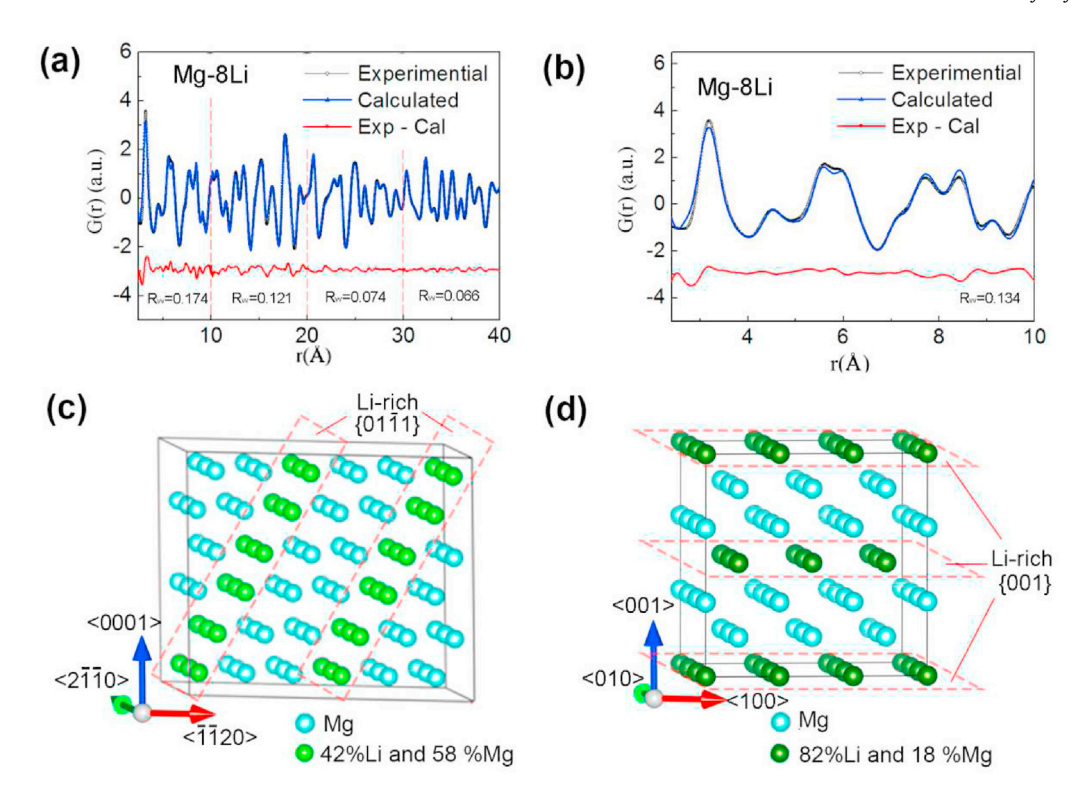


Fig. 2. SRO of Mg-8wt.%Li alloy. (a) Binary-phase neutron-diffraction PDF pattern fitted by a random atomic-occupancy model. (b) Fitting patterns of the binary Mg-8wt.%Li alloy of 2.4-10 Å with the best binary structure. Black line are the measured data, blue solid line is the calculated PDF of the best-fit structural models, and the red solid line is the differences. Schematic diagram of the best model derived from data fit, showing atom arrangements: (c) α-phase structure of the binary Mg-8wt.%Li alloy, and (d) β-phase structure of the binary Mg-8wt.%Li alloy. (For interpretation of the references to color in this figure legend, the reader is referred to the Web version of this article.)

4.2. Transformation of the Mg-Li alloy

First, the transformation elemental unit size of the Mg—Li alloy was calculated, assuming that the cells are cubic. The predicted diagonal length of a transformation-elemental unit was calculated by taking into account the periodic interface structure, i.e., $15.5~\text{Å} \times \sqrt{3} \approx 26.8~\text{Å}$. The transformation-elemental units need to have suitable element distributions with an appropriate configuration energy and configuration entropy in order to obtain a high enough Gibbs free energy [31]. This is the reason why SRO structures have formed with similar atom distributions in transformation-elemental units. The diagonal length of the SRO cell is about 20 Å, which compares fairly well with the diagonal length of the predicted transformation elemental unit (26.8 Å).

Then, the Li-atom distribution in most common SRO cells of α and β phases in the binary Mg–Li alloy was used to analyze the transformation process. The Li-atom distributions within α and β phases suggest that they can transform to each other by a BCC-HCP displacive model without the atom rearrangement proposed by Burgers [32,33] (Fig. 3). In this process, the set of $(\overline{211})_{\beta}$ planes can be obtained from the set of $(\overline{2}020)_{\alpha}$ planes by shearing the $(\overline{2}020)_{\alpha}$ planes in the $[11\overline{2}0]_{\alpha}$ direction and by expanding these planes in the $[11\overline{2}0]_{\alpha}$ direction. These results suggest that the α/β transformation in the binary Mg-Li could occur by an atomic-scale displacive process. The transformation process is controlled by the fluctuation of the Li-atom content within cells. The α phase cell becomes metastable when the Li-atom content within the cell reaches about 28%. Then a cell transformation occurs with the displacive process, which forms a cell of the β phase. A similar $\beta \rightarrow \alpha$ transformation will occur when the β phase has a Li content lower than about 18%. Similarly, the atomic displacive process of the bcchcp phase transformation with a nano-scale concentration modulation was observed in Ti alloys by Hao et al. [34,35]. This obvious non-uniform transformation process was also observed in the s-s transformation of colloidal crystals [36]. These observations imply that the atomic-scale displacive transformation process is an universal phenomenon in diffusional transformations.

5. Discussion

Fig. 4a shows the changes in the Gibbs free energy as a function of the precipitation length, l_n/D , based on Equations (4), (7) and (8). The synergistic effects of $\Delta G'_d$ and $\Delta G'_i$ on the phase transformation are depicted in Fig. 4b. Four cases for ΔG_d , are considered: $\overline{\Delta G_i'} > \Delta G_d' > \Delta G_i' \min$ (Case A), $\Delta G_d' = \overline{\Delta G_i'}$ (Case B), $\Delta G_i' \max > \Delta G_d' >$ $\overline{\Delta G'_i}$ (Case C), and $\Delta G'_d > \Delta G'_i$ max (Case D). The Gibbs free-energy curves have periodic energy barriers, which can shrink (ΔG_{sh}^T) and grow (ΔG_{gr}^{T}), see Fig. 4a. These energy barriers need to be overcome with thermal activation within a cell during transformation. Apparently, the energy barriers formed from the high energy interfacial atoms (red atoms in the bottom of Fig. 4b) prevent spontaneous and continuous transformation, when $\Delta G'_i \max > \Delta G'_d > \Delta G'_i \min$, leading to an atomic-scale thermallyactivated displacive transformation. In this process, the thermallyactivated diffusion of elements in a transformation cell is required to provide the extra driving force via the formation of the SRO structure. The intrinsic atomic-scale displacive transformation within a periodic cell is rendered as a reconstructive/diffusional transformation. The diffusional transformation is a special displacive transformation in which the transformation takes place through a displacive process within a cell unit.

The largest differential interfacial energy can be overcome when

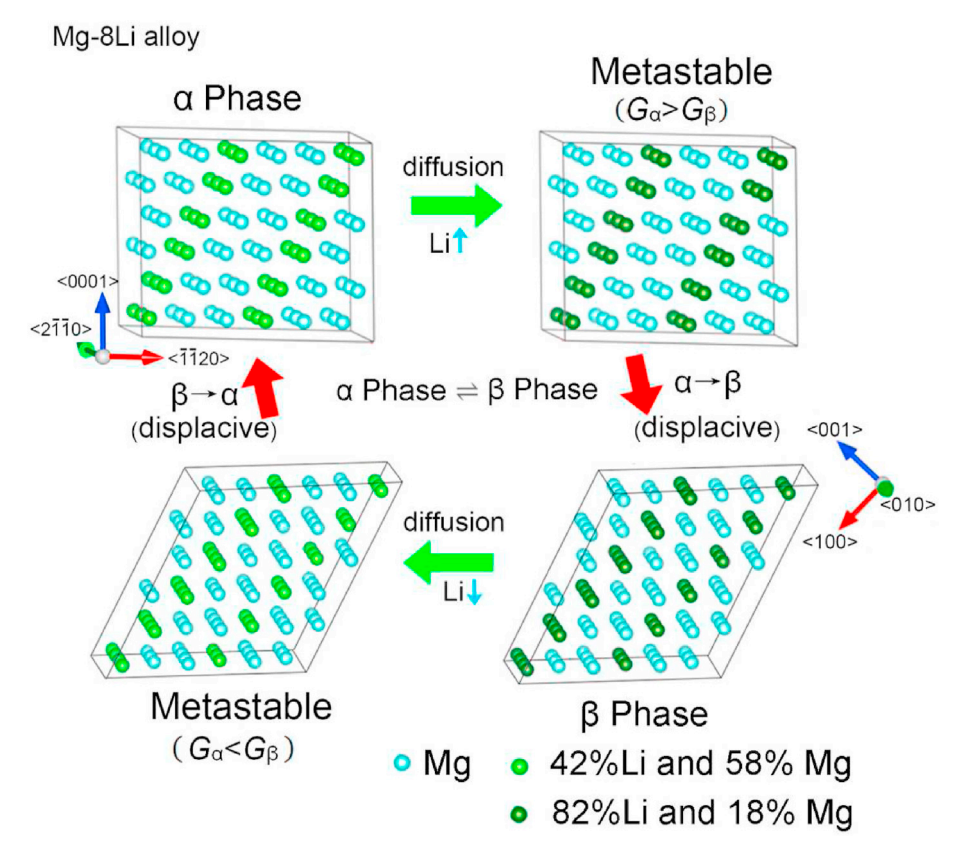


Fig. 3. Schematic of the effect of the Li atom content and atomic structure on the displacive transformation of the binary Mg–Li alloy. Based on the phase diagram for the Mg–Li alloy, the α phase forms when the Li content is lower than about 17 atomic percent (at.%) (the Li content of the green sites in the α phase are lower than 42 at.%), and the α phase transfers to the β phase when the Li content is higher than about 27 at.% (the Li content of green sites in the β phase are higher than 82 at.%). Therefore, the transformation-driving force is controlled by the fluctuation of the Li atom content within cells. Thus, the α -phase cell becomes metastable, when the Li atom content within the cell reaches about 27 at.%, then a cell transformation occurs with the displacive process and forms a cell of the β phase. And a similar $\beta \to \alpha$ transformation will occur when the β phase obtains the Li content lower than about 17 at.%. (For interpretation of the references to color in this figure legend, the reader is referred to the Web version of this article.)

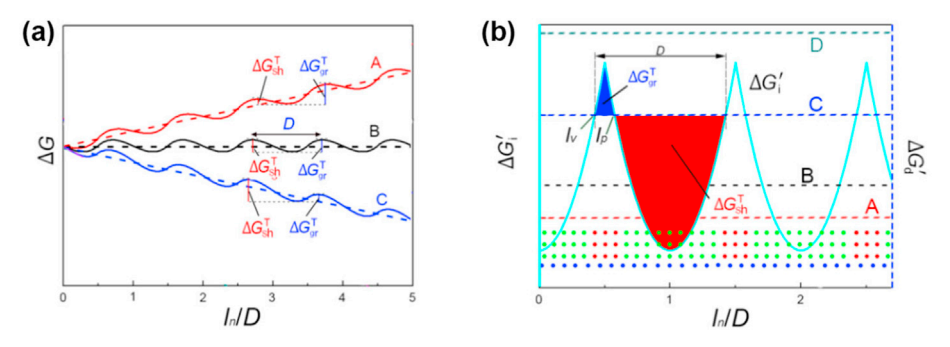


Fig. 4. The effect of the periodic interfacial energy on the transformation process. (a) Gibbs free energy-transformation length for different driving forces, as plotted from the differential interfacial energy-transformation model. Three cases for $\Delta G_{\rm d}'$ are indicated with $\overline{\Delta G_i'} > \Delta G_{\rm d}' > \Delta G_{\rm i}'$ min (Case A), $\Delta G_{\rm d}' = \overline{\Delta G_i'}$ (Case B), and $\Delta G_{\rm i}'$ max > $\Delta G_{\rm d}' > \overline{\Delta G_i'}$ (Case C). ΔG curves of CNT with the same driving force but considering the interfacial energy as a constant are shown as short dash lines of the same color. (b) $\Delta G_i'$ and $\Delta G_{\rm d}'$ vs. transformation length for different driving forces, where the crosses, I_p and I_v , represent the transformation lengths of the wave peak and valley of ΔG , respectively. Case D is for the $\Delta G_i'$ greater than the $\Delta G_i'$ max. The red, green, and blue atoms are high energy interfacial atoms, low energy interfacial atoms, and parent phase atoms, respectively. (For interpretation of the references to color in this figure legend, the reader is referred to the Web version of this article.)

a system has a high enough $\Delta G_{\rm d}'$ (case D), which is greater than $\Delta G_{\rm i}'$ max. Under this condition, the transformation can take place monotonically as a displacive transformation. When the interface is completely coherent, the periodic interface atom misfit does not hold, and the transformation can take place spontaneously and continuously, since there is no periodic barrier. Hence, the traditional displacive transformation occurs.

The common characteristics in the structures of any singular

interface are their periodicity in three dimensions [2,37,38]. Their periodic misfit mainly depends on the interface orientation and lattice parameters between the new and parent phases [39]. Depending on the anisotropy of the periodic interface energy along different orientations, the new phase can grow into various macrostructures with various interface morphologies.

6. Conclusions

In summary, we have introduced the effect of the differential phase interfacial energy of each atom layer on a phase transformation to explain the relationship between displacive and diffusional transformations and analyzed the effect of the periodic energy barriers on the transformation behavior. We have found that the diffusional transformation with SRO is strictly an atomic-level displacive transformation, whereas the nature of displacive and diffusional transformations are displacive processes with different driving forces. The present work makes an important step towards building a unified theory of the s-s transformations and suggest a novel method for analyzing the transformation process.

Credit author statement

Ye Cui: Conceptualization, Methodology, Writing — original draft, Resources, Formal analysis. **Yang Zhang**: Formal analysis. **Lixin Sun**: Formal analysis. **Mikhail Feygenson**: Formal analysis. **Mingyu Fan**: Resources. **Xun-Li** Wang: Formal analysis. **Peter K. Liaw**: Writing — review & editing. **Ian Baker**: Writing — review & editing. **Zhongwu Zhang**: Conceptualization, Methodology, Supervision, Resources, Writing — review & editing, Formal analysis.

Declaration of competing interest

The authors declare that they have no known competing financial interests or personal relationships that could have appeared to influence the work reported in this paper.

Acknowledgements

The present work was supported by the National Key R & D Project (2018YFE0115800), the NSFC Funding (U2141207, 52001083, 52171111), China Postdoctoral Science Foundation Funded Project (2019T120255), Natural Science Foundation of Heilongjiang (LH2019E030), and Heilongjiang Touyan Innovation Team Program. A portion of the present research at the Oak Ridge National Laboratory's Spallation Neutron Source (SNS) was sponsored by the Scientific User Facilities Division, Office of Basic Energy Sciences, U.S. Department of Energy. The use of the Advanced Photon Source at the Argonne National Laboratory was supported by the U.S. Department of Energy, Office of Science, Office of Basic Energy Sciences, under Contract No. DE-AC02-06CH11357. P. K. L. very much appreciates the supports from the National Science Foundation (DMR-1611180 and 1809640) with program directors, Drs. J. Yang, G. Shiflet, and D. Farkas. I.B. was supported by the U.S. Department of Energy, Office of Science, Basic Energy Sciences, under Award # DE-SC0018962. We thank Profs. William D. Nix, John Perepezko, and Lindsay L. Greer for help with critical reading of the manuscript.

Appendix A. Supplementary data

Supplementary data to this article can be found online at https://doi.org/10.1016/j.mtphys.2022.100668.

References

- M.X. Zhang, P.M. Kelly, Crystallographic features of phase transformations in solids, Prog. Mater. Sci. 54 (2009) 1101–1170, https://doi.org/10.1016/ j.pmatsci.2009.06.001.
- [2] W.Z. Zhang, G.C. Weatherly, On the crystallography of precipitation, Prog. Mater. Sci. 50 (2005) 181–292, https://doi.org/10.1016/j.pmatsci.2004.04.002.
- [3] H. Zhou, L. Wu, H.Q. Wang, J.C. Zheng, L. Zhang, K. Kisslinger, Y. Li, Z. Wang, H. Cheng, S. Ke, Y. Li, J. Kang, Y. Zhu, Interfaces between hexagonal and cubic

- oxides and their structure alternatives, Nat. Commun. 8 (2017) 1474, https://doi.org/10.1038/s41467-017-01655-5.
- [4] S. Jiang, H. Wang, Y. Wu, X. Liu, H. Chen, M. Yao, B. Gault, D. Ponge, D. Raabe, A. Hirata, M. Chen, Y. Wang, Z. Lu, Ultrastrong steel via minimal lattice misfit and high-density nanoprecipitation, Nature 544 (2017) 460–464, https:// doi.org/10.1038/nature22032.
- [5] T.M. Smith, B.D. Esser, N. Antolin, A. Carlsson, R.E.A. Williams, A. Wessman, T. Hanlon, H.L. Fraser, W. Windl, D.W. McComb, M.J. Mills, Phase transformation strengthening of high-temperature superalloys, Nat. Commun. 7 (2016) 13434. https://doi.org/10.1038/ncomms13434.
- [6] T. Irifune, A. Kurio, S. Sakamoto, T. Inoue, H. Sumiya, Materials ultrahard polycrystalline diamond from graphite, Nature 421 (2003) 599–600, https:// doi.org/10.1038/421599b.
- [7] Z. Li, K.G. Pradeep, Y. Deng, D. Raabe, C.C. Tasan, Metastable high-entropy dual-phase alloys overcome the strength-ductility trade-off, Nature 534 (2016) 227–230. https://doi.org/10.1038/nature17981.
- [8] H. Chen, Y.D. Wang, Z. Nie, R. Li, D. Cong, W. Liu, F. Ye, Y. Liu, P. Cao, F. Tian, X. Shen, R. Yu, L. Vitos, M. Zhang, S. Li, X. Zhang, H. Zheng, J.F. Mitchell, Y. Ren, Unprecedented non-hysteretic superelasticity of 001 -oriented NiCoFeGa single crystals, Nat. Mater. 19 (2020) 712–718, https://doi.org/10.1038/s41563-020-0645-4.
- [9] S. Mori, S. Hatayama, Y. Shuang, D. Ando, Y. Sutou, Reversible displacive transformation in MnTe polymorphic semiconductor, Nat. Commun. 11 (2020) 85, https://doi.org/10.1038/s41467-019-13747-5.
- [10] D.A. Porter, K.E. Easterling, M.Y. Sherif, Phase Transformation in Metals and Alloys. CRC Press. 2009.
- [11] J.W. Christian, Lattice correspondence, atomic site correspondence and shape change in "diffusional-displacive" phase transformations, Prog. Mater. Sci. 42 (1997) 101–108, https://doi.org/10.1016/S0079-6425(97)00009-1.
- [12] M. Hillert, Paradigm shift for bainite, Scripta Mater 47 (2002) 175–180, https://doi.org/10.1016/s1359-6462(02)00125-2.
- [13] F.G. Caballero, M.K. Miller, C. Garcia-Mateo, J. Cornide, M.J. Santofimia, Temperature dependence of carbon supersaturation of ferrite in bainitic steels, Scripta Mater 67 (2012) 846–849, https://doi.org/10.1016/j.scriptamat.2012.08.007.
- [14] S.E. Offerman, N.H. van Dijk, J. Sietsma, S. Grigull, E.M. Lauridsen, L. Margulies, H.F. Poulsen, M.T. Rekveldt, S. van der Zwaag, Grain nucleation and growth during phase transformations, Science 298 (2002) 1003–1005, https:// doi.org/10.1126/science.1076681.
- [15] L. Bourgeois, Y. Zhang, Z. Zhang, Y. Chen, N.V. Medhekar, Transforming solid-state precipitates via excess vacancies, Nat. Commun. 11 (2020) 1248, https://doi.org/10.1038/s41467-020-15087-1.
- [16] Y.C. Lin, D.O. Dumcencon, Y.S. Huang, K. Suenaga, Atomic mechanism of the semiconducting-to-metallic phase transition in single-layered MoS2, Nat. Nanotechnol. 9 (2014) 391–396, https://doi.org/10.1038/nnano.2014.64.
- [17] M.V. Kral, B.C. Muddle, J.F. Nie, Crystallography of the bcc/hcp transformation in a Mg-8Li alloy, Mat. Sci. Eng a-Struct. 460 (2007) 227–232, https://doi.org/ 10.1016/j.msea.2007.01.102.
- [18] H.W. Sheng, W.K. Luo, F.M. Alamgir, J. Bai, E. Ma, Atomic packing and short-to-medium-range order in metallic glasses, Nature 439 (2006) 419–425, https://doi.org/10.1038/nature04421.
- [19] N. Zhang, H. Yokota, A.M. Glazer, D.A. Keen, S. Gorfman, P.A. Thomas, W. Ren, Z.-G. Ye, Local-scale structures across the morphotropic phase boundary in PbZr_{1-x}Ti_xO₃, lucrj 5 (2018) 73–81, https://doi.org/10.1107/s2052252517016633.
- [20] K. Xiang, W. Xing, D.B. Ravnsbaek, L. Hong, M. Tang, Z. Li, K.M. Wiaderek, O.J. Borkiewicz, K.W. Chapman, P.J. Chupas, Y.M. Chiang, Accommodating high transformation strains in battery electrodes via the formation of nanoscale intermediate phases: operando investigation of olivine NaFePO₄, Nano Lett. 17 (2017) 1696–1702, https://doi.org/10.1021/acs.nanolett.6b04971.
- [21] S.D.M. Jacques, M. Di Michiel, S.A.J. Kimber, X. Yang, R.J. Cernik, A.M. Beale, S.J.L. Billinge, Pair distribution function computed tomography, Nat. Commun. 4 (2013) 3536, https://doi.org/10.1038/ncomms3536.
- [22] J. Neuefeind, M. Feygenson, J. Carruth, R. Hoffmann, K.K. Chipley, The nanoscale ordered materials diffractometer NOMAD at the spallation neutron source SNS, Nucl. Instrum. Methods B 287 (2012) 68–75, https://doi.org/ 10.1016/j.nimb.2012.05.037.
- [23] X. Qiu, J.W. Thompson, S.J.L. Billinge, PDFgetX2: a GUI-driven program to obtain the pair distribution function from X-ray powder diffraction data, J. Appl. Crystallogr. 34 (2004), https://doi.org/10.1107/S0021889804011744, 678-678
- [24] C.L. Farrow, P. Juhas, J.W. Liu, D. Bryndin, E.S. Bozin, J. Bloch, T. Proffen, S.J.L. Billinge, PDFfit2 and PDFgui: computer programs for studying nanostructure in crystals, J Phys-Condens. Mat. 19 (2007), https://doi.org/10.1088/ 0953-8984/19/33/335219.
- [25] S.Y. Zhou, C. Deng, S.F. Liu, Y.H. Liu, J.L. Zhu, X.L. Yuan, Microstructure, texture, and fracture of pure magnesium adiabatic shear band under high strain rate compression, Mat. Sci. Eng. a-Struct. 822 (2021), https://doi.org/10.1016/j.msea.2021.141632.
- [26] J.D. Eshelby, The determination of the elastic field of an ellipsoidal inclusion, and related problems, in: Proceedings of the Royal Society A vol. 241, 1957, pp. 376–396, https://doi.org/10.1098/rspa.1957.0133.
- [27] J.F. Nie, Crystallography and migration mechanisms of planar interphase boundaries, Acta Mater 52 (2004) 795–807, https://doi.org/10.1016/ j.actamat.2003.10.019.

- [28] Y. Zou, J. Li, H. Wang, K. An, M. Zhang, D. Chen, Z. Zhang, Deformation mode transition of Mg-3Li alloy: an in situ neutron diffraction study, J. Alloys Compd. 685 (2016) 331–336, https://doi.org/10.1016/j.jallcom.2016.05.310.
- [29] L. Reinhard, B. Schonfeld, G. Kostorz, W. Buhrer, Short-range order in α-brass, Phys. Rev. B 41 (1990) 1727–1734, https://doi.org/10.1103/ PhysRevB.41.1727.
- [30] I. Mirebeau, G. Parette, Neutron study of the short range order inversion in Fe_{1-x}Cr_x, Phys. Rev. B 82 (2010) 104203, https://doi.org/10.1103/ PhysRevB.82.104203.
- [31] J.M. Cowley, An approximate theory of order in alloys, Phys. Rev. 77 (1950) 669–675, https://doi.org/10.1103/PhysRev.77.669.
- [32] W.G. Burgers, On the process of transition of the cubic-body-centered modification into the hexagonal-close-packed modification of zirconium, Phys. Nonlinear Phenom. 1 (1934) 561–586, https://doi.org/10.1016/S0031-8914(34)80244-3.
- [33] F.M. Wang, R. Ingalls, Iron bcc-hcp transition: Local structure from x-rayabsorption fine structure, Phys. Rev. B 57 (1998) 5647–5654, https://doi.org/ 10.1103/PhysRevB.57.5647.
- [34] H.L. Wang, Y.L. Hao, S.Y. He, K. Du, T. Li, E.G. Obbard, J. Hudspeth, J.G. Wang,

- Y.D. Wang, Y. Wang, F. Prima, N. Lu, M.J. Kim, J.M. Cairney, S.J. Li, R. Yang, Tracing the coupled atomic shear and shuffle for a cubic to a hexagonal crystal transition, Scripta Mater. 133 (2017) 70–74, https://doi.org/10.1016/j.scriptamat.2017.02.024.
- [35] Y.L. Hao, D.L. Gong, T. Li, H.L. Wanga, J.M. Cairney, Y.D. Wang, E.G. Obbard, F. Sun, F. Prima, S.J. Li, K. Du, R. Yang, Continuous and reversible atomic rearrangement in a multifunctional titanium alloy, Materialia 2 (2018) 1–8, https://doi.org/10.1016/j.mtla.2018.08.013.
- [36] Y. Peng, F. Wang, Z. Wang, A.M. Alsayed, Z. Zhang, A.G. Yodh, Y. Han, Two-step nucleation mechanism in solid-solid phase transitions, Nat. Mater. 14 (2015) 101–108. https://doi.org/10.1038/nmat4083.
- [37] J.M. Rigsbee, H.I. Aaronson, A computer modeling study of partially coherent f.c.c.:b.c.c. boundaries, Acta Metall 27 (1979) 351–363, https://doi.org/ 10.1016/0001-6160(79)90028-2.
- [38] P.M. Kelly, M.X. Zhang, Edge-to-edge matching the fundamentals, metall mater, OR Trans. 37A (2006) 833–839, https://doi.org/10.1007/s11661-006-0056-4.
- [39] J.M. Howe, Interfaces in Materials, John Wiley and Sons, New York, 1997.